

EVS27
Barcelona, Spain, November 17-20, 2013

System Integration and Power Flow Management for the Engine-Generator Operation of a Range-extended Electric Vehicle

Chang Chih-Ming¹, Yang Kuang-Shine²

¹*Metal and processing R&D department, Metal Industries R&D Centre, 1001 Kaonan Highway, Kaohsiung, Taiwan 81160, c-ming@mail.mirdc.org.tw*

²*Metal and processing R&D department, Metal Industries R&D Centre, 1001 Kaonan Highway Kaohsiung, Taiwan 81160, yangks@mail.mirdc.org.tw*

Abstract

This paper introduced a new power flow control strategy for a variable speed engine-generator based range-extended electric vehicle. The specific fuel consumption map of the internal combustion engine (ICE) has been obtained by off-line experiments to achieve optimal fuel efficiency. Finally, a typical range-extended electric vehicle is modeled and investigated such as acceleration traversing ramp, maximum speed and fuel consumption are performed on the dynamic model of a range-extended electric vehicle. The goal of this paper was to obtain a complete and optimum control structure for the studied range extended electric vehicle. Numerical models of battery and transmission were established. In order to check the model and control of the studied system, a simple strategy is taken into account and discussed the programs were written base on these theories. At the end of this paper, simulation results were analyzed, and it has been proved that range-extended electric vehicle can avoid deep discharge cycles. Therefore, range extended electric vehicle battery cycle life definitely greater than EV battery cycle life. It's also meaning that battery operating cost of range extended electric vehicle being much lower than EV.

Keywords: System Integration, Power Flow, Range-extended Electric Vehicle

1 Introduction

As fossil fuel energy sources become more and more scarce, technologies that show the potential for decreasing energy use and air pollution are being evaluated. One such new technology in the field of transportation is the hybrid vehicles. The hybrid electric vehicle propulsion system is categorized into two types [1], one is a series hybrid and the other one is parallel hybrid. Unlike the conventional HEV, plug-in hybrid electric vehicles (PHEV) are essentially hybrid

electric vehicles with batteries that can be recharged by plugging into a standard electric power outlet. A PHEV powertrain consists of electrical components including electric motors, an energy storage system, and power electronic converters and also mechanical components like an internal combustion engine (ICE). The ICE provides the vehicle an extended driving range while the electric motor increases efficiency and fuel economy by regenerating energy during braking and storing excess energy from the ICE during coasting, so the driver does not have to worry about running out of electric power as in an

electric vehicle (EV). The reported fuel economy of PHEV prototypes ranges from 60 to 150 miles per gallon (mpg) [2], is defined as the distance which the vehicle can travel only by using its electric motor and batteries in which during this period the engine is off, resulting in zero fuel consumption and zero emissions. In any PHEV architecture, the battery plays an important role in the powertrain. The electric energy stored in the battery is obtained either from the electric grid, the gasoline engine through a generator, or regenerative braking. [3] In order to utilize best energy management strategies various researches for series HEVs have tried to get optimal fuel efficiency. In paper [4] proposes an optimal control strategy of the engine-generator subsystem to generate a desired amount of energy within a given period of time. The optimization algorithm, based on trajectory optimization, determines the torque and speed reference signals for the engine-generator subsystem that achieve maximum efficiency. In the paper [5] presents a power flow control strategy for series hybrid electric vehicle. The proposed power flow controller makes it possible that the ICE operates at its optimal fuel efficiency points without degrading desired dynamic performance. To get better fuel economy and vehicle performance, the paper [6] design and sizing of its powertrain components has the optimal sizing of an SHEV. The SHEV after optimization has better fuel economy than that of the original one. The paper [7], the application of batteries and ultracapacitors in electric energy storage units for battery powered (EV) and charge sustaining and plug-in hybrid-electric (HEV and PHEV) vehicles have been studied in detail. The use of IC engines and hydrogen fuel cells as the primary energy converters for the hybrid vehicles was considered. The study focused on the use of lithium-ion batteries and carbon/carbon ultracapacitors as the energy storage technologies most likely to be used in future vehicles. According to the same study the paper [8] this paper investigated the relationships between vehicle cost, mass total range, and battery pack mass. The mass compounding effect for battery electric vehicles was investigated and found to be of significant importance to understand the system integration of battery electric technology. In the paper [9], global methodology together with a detailed analysis of the impact of different types of powertrains EMs, namely, PMSM drive and IM drive, in different drive cycles for typical daily

EV use (ECE-15, NEDC and 50-km/h fixed speed), is presented. In the paper [10], the plug-in vehicle has a modular topology where different solutions for the battery-power converter electric machine chain of a plug-in electric vehicle are possible to be simulated. In the simulation results of a solution for this electric chain allowing bi-directional power flow and using different types of batteries is presented and analyzed.

In this paper, a range-extended electric vehicle (RE-EV) utilizing a gasoline engine as a main energy source and a battery module as an energy storage element is discussed. This paper presents a methodology of calculating the optimal torque and speed commands for the engine-generator system of a range-extended electric vehicle. According to all electric range control strategy, a model of range-extended electric vehicle was built, which was used for simulation the energy consumption and cost were compared to tradition range-extended electric vehicle. Finally, to verify the presented power flow management algorithm, the proposed power-flow management algorithm has been experimentally verified with a full-scale prototype vehicle (C segment).

2 Structural characteristics of range-extended electric vehicle

The engine in the range-extended electric vehicle is not directly linked to the transmission for driving wheels but connected to the generator for electricity production. Its overall architecture is presented in Figure 1. The model provides an accurate description of a range-extended electric vehicle in Simulink, including consideration for transient behavior. The powertrain contains IM motor connected to a three-phase inverter which is driven by a Genset system and battery system. The Genset system of energy consists of a 1.0L gasoline engine and a Permanent Magnet Synchronous Generator (PMSG) connected to a three-phase rectifier. The battery system consists of a Li-PO battery connected to a bi-directional DC-DC converter (Fig. 2). The motor system (IM and inverter), the Genset system and the battery system are all connected to a DC bus where the power transfer occurs. In the case of regenerative braking, the Genset system is turned off and IM motor to capture the energy from the wheels and convert it to electric energy and store it into the battery.

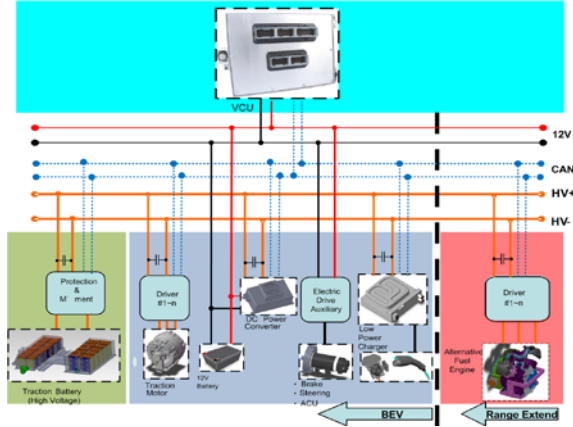


Figure1: Overview of the architecture of the modeled range-extended electric vehicle



Figure2: DC-DC converter

3 Vehicle Dynamic Modeling

Issues relating to performance and range in electric vehicle is very important. The first step in vehicle performance modeling is to produce an equation for the tractive effort. This is the force propelling the vehicle forward, transmitted to the ground through drive wheels. Equation 1 shows that the tractive effort can be reduce into four main categories, the rolling resistance force $F_{rolling}$ due to friction of the vehicle tires on the road, the aerodynamic drag force F_{aero} caused by the friction of the body moving through the air, overcoming the current vehicle state of motion $F_{inertia}$, and finally the grade or inclination that the vehicle is travelling on F_{grade} . Figure 3 shows a physical representation of the forces as they affect the vehicle during motion. The total tractive effort is equal to F_{tr} and the sum of the resistive forces in the x-direction accounted for in equation 1.

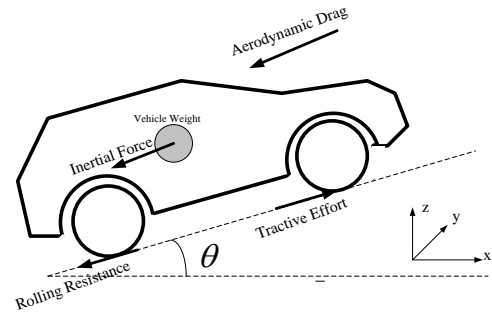


Figure3: Vehicle Dynamic

$$F_{tr} = F_{rolling} + F_{aero} + F_{grade} + F_{inertia} \quad (1)$$

Equations 2 through 5 express the different terms making up the tractive effort equation. The parameter C_{rr0} is the coefficient of rolling resistance, C_{rr1} is the coefficient of rolling resistance affected by Velocity, m is vehicle mass, g is the acceleration due to gravity, ρ is the density of air, C_D is aero-dynamic drag coefficient, A_f is the frontal area of the vehicle, V is vehicle velocity, M_i is an inertial mass factor term to account for the rotating inertia of the wheels, tires, and other rotating components, dV/dt is the acceleration from one time step to the next for the drive cycle, and θ (related to grade) is the angle of incline. For normal inclines, the $\sin(\theta)$ term that could be included in Equation 4 is approximated as 1. The variables are summarized in Table 1.

$$F_{rolling} = C_{rr0}mg + C_{rr1}mgV \quad (2)$$

$$F_{inertia} = mM_i \frac{dV}{dt} \quad (3)$$

$$F_{grade} = mg \sin(\theta) \quad (4)$$

$$F_{aero} = \frac{1}{2} \rho C_D A_f V^2 \quad (5)$$

Table1: Vehicle Parameter

| | | |
|-----------|--|----------|
| C_{rr0} | Static Coefficient of rolling resistance | [-] |
| C_{rr1} | Moving coefficient of rolling resistance | [-] |
| m | Vehicle mass | kg |
| g | Gravity | m/s^2 |
| V | Velocity | m/s |
| ρ | Density of air | kg/m^3 |
| C_D | Coefficient of Drag | [-] |
| A_f | Frontal Area | m^2 |
| M_i | Inertia mass factor | [-] |
| dV/dt | Drive cycle acceleration | m/s^2 |
| θ | Degree of inclination | [-] |

The rolling resistance term is always present when the vehicle is in motion. Aerodynamic drag force increases with the square of velocity, so with

higher speeds comes more drag on the vehicle. The inertia term is dependent on vehicle acceleration rate, and will sum to zero for a drive cycle that starts and ends at zero speed. Grade, while not always present, does have an impact on the energy required to complete a drive cycle, and if present, should be accounted for.

4 Motor and Transmission Box

Choosing normal rated power of motor correctly is very important, because too low the motor would be overloaded all the time and too high the motor would run under low load. If the motor always runs under low load, its efficiency and power factor would decrease leading to a waste of electricity and an increase of the capacity of power battery. Due to the simple and rugged construction, low cost and maintenance, high performance and sufficient starting torque and good ability of acceleration, induction motor is one of the well suited motors for the electric propulsion systems. We used the efficiency maps for the motor and inverter of this system are shown in Figure 6 and Figure 7 which represents the steady state characteristics related with the motor speed and torque. The motor with a working power range rating equal to or greater than the power range calculated for the vehicle dynamic from equation 1. The factors involved in computing the power are: the tire torque, the vehicle speed, tire's rotations per mile, and overall drive-train-efficiency. The motor driver is shown in Figure 5, which requires IGBT switches and diodes per phase. The switches and diodes must be rated to withstand the supply voltage plus any high current overload. Here in the circuit, IGBT switch is used because of its high input impedance as in a MOSFET, and low conduction losses similar to BJT. This circuit is capable of operating the machine as a motor and a generator.



Figure4: IM motor

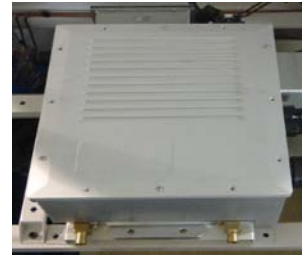


Figure5: inverter

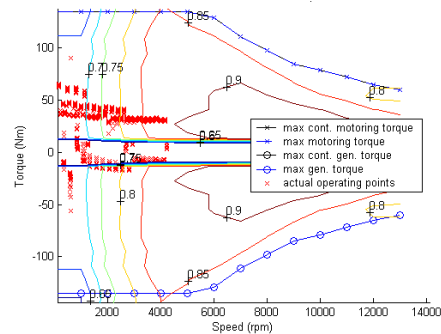


Figure6: efficiency maps (I)

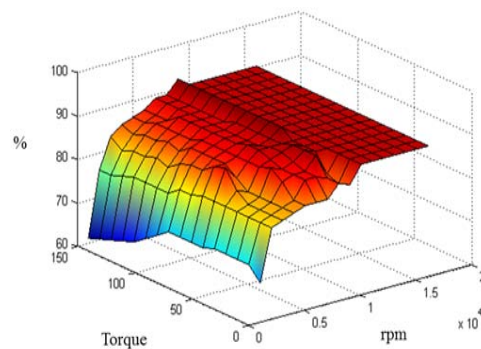


Figure7: efficiency maps (II)

To satisfy the highest speed, greatest grad ability, and accelerating time as planned, the selection of gear ratio of drive line system is crucial. The selection of gear ratio would be based on two alternatives, single gear or multiple gears, according to the existing design concept. This design requirement is mainly based on the chosen motor performance and car performance. For instance, if the chosen motor could meet the performance requirement and its governing range is sufficient, then a gear box with constant speed ratio could be used directly. The use of gear box with single gear ratio could not only decrease the weight and size of electric car, but also promote drive efficiency and lower the cost. Its specifications are as follows:

- (1) Upper limit of gear ratio of drive line system:
The upper limit of drive line system ratio is mainly decided by the highest rotational speed of the

motor (n_m) and the required highest vehicle velocity (v_m), so it can be illustrated as

$$G_H \leq \frac{0.377n_m r}{v_m} \quad (6)$$

$$G_H = i_0 \times i_g \quad (7)$$

Where

r is wheel radius

i_0 is differential ratio

i_g is transmission ratio

From the above formula, one can know that if the wheel size is fixed, the relationship of motor speed and car speed with different gear ratio is shown in the following Figure 8. The diagram shows that if the motor speed is consistent, lower gear ratio would result in higher corresponding car speed; if driving resistance has to be overcome, then motor output torque must be increased if the gear ratio is lower.

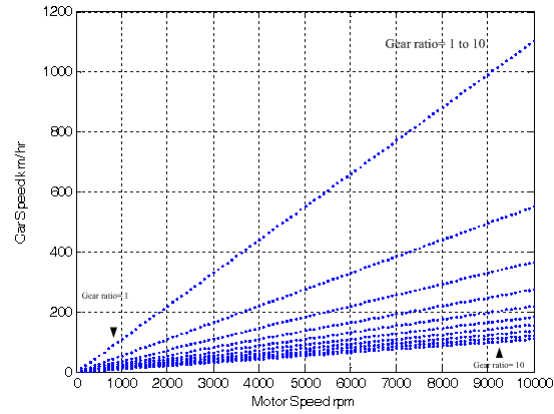


Figure8: Car speed with different gear ratio

(2) Lower limit of gear ratio of drive line system: For lower limit of gear ratio of drive line system, the maximum value of gear ratio of drive line system could be calculated using the following two formulas. Drive ration should always be selected based on attaining the vehicle tractive effort and vehicle speed specifications. The lower limit of drive ratio of drive line system is decided according to the corresponding output torque (T_{nm}) of the highest motor speed and corresponding driving resistance (F_{nm}) of the highest car speed (v_m)

$$G_L \geq \frac{F_{nm} r}{\eta_t T_{nm}} \quad (8)$$

where

r is wheel radius

η_t is drive efficiency

$$F_{nm} = c_{rr0} mg + c_{rr1} mg v_m + \frac{1}{2} \rho C_D A_f v_m^2 \quad (9)$$

$$T_{nm} = 9549 \frac{P_e}{n_m} \quad (10)$$

Figure 9 shows the corresponding motor output torque demand relationship under fixed wheel size, different gear ratio, and same driving resistance. It shows that under consistent driving resistance, the corresponding output torque (T_{nm}) is higher if the corresponding highest motor speed of gear ratio is smaller.

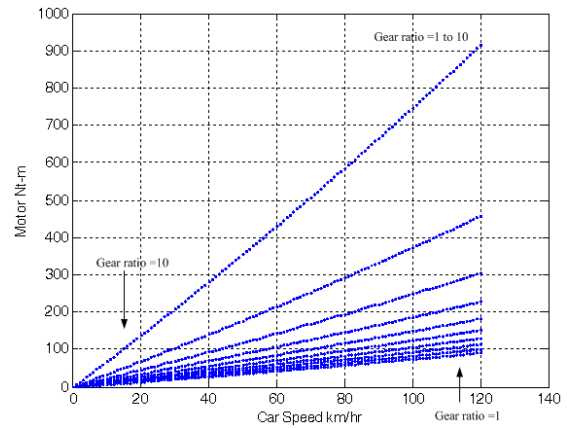


Figure9: Motor output torque and different gear ratio

The lower limit of gear ratio of drive line system is decided according to the highest motor output torque (T_{am}) and corresponding driving resistance (F_{nm}) of highest climbing angle (θ)

$$G_{La} \geq \frac{F_{am} r}{\eta_t T_{nm}} \quad (11)$$

Where

$$F_{am} = mg \sin(\theta) + \frac{1}{2} \rho C_D A_f v_\alpha^2 + c_{rr0} mg + c_{rr1} mg v_\alpha \quad (12)$$

v_α is the corresponding car speed km/hr of highest climbing angle. In this paper the selection of gear ratio would be single gear (1:10) are show as follow Figure 10.



Figure10: Transmission box

5 Battery System

The power a high voltage battery is able to provide varies with SOC, temperature, and battery life. In order to provide more accurate battery power limits as it ages a method of estimating battery power capabilities needs to be developed, which allows the vehicle controls to maximize its power capabilities and to provide drivers best performance and fuel economy and protection of high voltage battery system. The battery considered in this paper is of the Li-PO type for which a simplified version of the RC battery model is used. The RC battery model is shown in Figure 11 which consists of two capacitors C_c, C_b . The surface capacitor C_c has a small capacitance and mostly represents the surface effects of a cell. The capacitor C_b is called bulk capacitor, which has a very large capacitance and represents the ample capability of the battery to store charge chemically. The capacitor SOC can be determined by the voltage across the bulk capacitor. Three resistors R_t, R_e, R_c where R_t is called terminal resistor, R_e is called end resistor and R_c capacitor resistor, respectively.

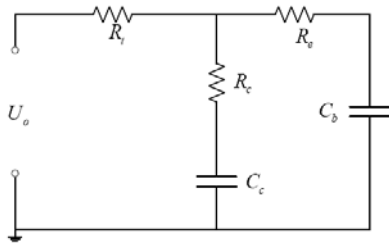


Figure11: RC battery model

For above RC battery model, the state-space equations are described as follows:

$$\begin{bmatrix} \dot{V}_{Cb} \\ \dot{V}_{Cc} \end{bmatrix} = \begin{bmatrix} -1 & 1 \\ C_b(R_e + R_c) & C_b(R_e + R_c) \\ 1 & -1 \\ C_c(R_e + R_c) & C_c(R_e + R_c) \end{bmatrix} \begin{bmatrix} V_{Cb} \\ V_{Cc} \end{bmatrix} \quad (13)$$

$$\begin{aligned} & + \begin{bmatrix} -R_c \\ C_b(R_e + R_c) \\ -R_e \\ C_c(R_e + R_c) \end{bmatrix} [I] \\ V_o & = \begin{bmatrix} R_c & R_e \\ (R_e + R_c) & (R_e + R_c) \end{bmatrix} \begin{bmatrix} V_{Cb} \\ V_{Cc} \end{bmatrix} \\ & + \left[-R_t - \frac{R_e R_c}{(R_e + R_c)} \right] [I] \end{aligned} \quad (14)$$

where V_{Cb} are the voltage of the bulk capacitor and V_{Cc} are the voltage of the surface capacitor,

respectively. I denote the output current and V is output voltage. The discharge process is denote the positive current. The parameters of the battery are tabulated in Table 2. Although these vary according to the temperature, energy level and current magnitude, parameters in the nominal condition are sufficient in the designing phase. On a battery pack level, the Li-PO modules are connected in a series combination to form a 300 to 350 V battery pack system for RE-EV application. Li-PO battery pack is equipped with a BMS system. This design of the BMS system improves the safety and the reliability of the battery system. The battery pack is show in Figure 12.



Figure12: Battery pack

The battery was simulated using a capacitor in series with an internal resistance and a battery management system that monitors the SOC of the battery as shown in Figure 12. The following equations are used to calculate the SOC.

$$Q_T = CV \quad (15)$$

$$SOC = (Q_T - \int_0^t i(\tau) d\tau) / Q_T \quad (16)$$

where Q_T is the theoretical capacity of the battery, C is the capacitance, V is the battery voltage, and i is the output current of the battery.

Table2: Parameters of the battery

| No | Item | Rated Performance | Remark |
|----|----------------------------|---|---|
| 1 | Nominal Capacity | 50Ah/module (and 17Ah/cell) | Discharge: 0.5C, cut off voltage: 2.0V |
| 2 | Nominal Voltage | 3.2V | |
| 3 | Discharge Cut-off Voltage | 2.0V | |
| 4 | Charge Voltage | 3.65V | |
| 5 | Standard Charge Current | 0.5C (25A) | |
| 6 | Max. Charge current (A) | 3C (150A) | 3C (continue) |
| 7 | Max. Discharge current (A) | 5C (250A) | 5C (continue) |
| | | 10C (500A) | 10C (pulse 30secs) |
| 8 | Internal Resistance | 2mΩ(max.) | AC 1kHz |
| 9 | Weight (Approx.) | ≤ 1400 g | |
| 10 | Operating Temp. | Charge: 0°C ~45°C Discharge: -10°C ~60°C | Storage Temp. -10°C ~45°C |
| 11 | Battery Size | 155mm*135mm*36mm | |
| 12 | Specific Power | >1143W/Kg | (500A* 3.2V)/1.4Kg |
| 13 | Cycle Life | ≥ 2000 times | 0.5CCh./Disch. after 2000 times, >80% of initial capacity |
| 14 | Self-Discharge(Monthly) | < 2% | 23±2°C |

Figure 13, 14 and 15 below shows the real time measured terminal voltage and current for one cell, discharged at constant currents of 10A. Rated capacity (C) is 50Ah (10 hours at 1/5C-rate (30min)

discharge). Common practice is to normalize currents to the rated capacity (C) of the battery, so these data are measured at rates of 0.2C. The curves feature a fairly linear drop in voltage during discharge until the effective capacity is reached, at which time the voltage (2.2V) declines rapidly.

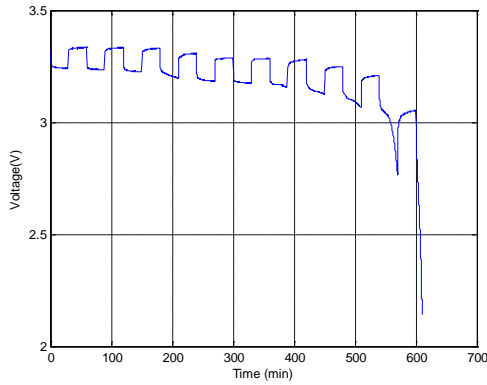


Figure13: Battery voltage (One Cell)

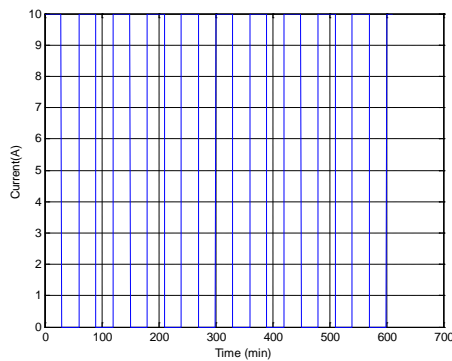


Figure14: Battery current (One Cell)

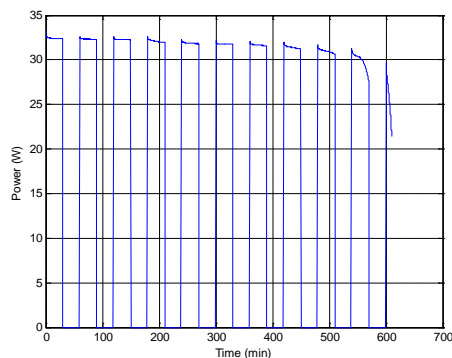


Figure15: Battery power (One Cell)

6 Genset System

The Power Generator control system is consist of physical system model including the engine, inverter, and generator, over speed protection module, PI controller, and engine map. Figure 16

shows the power and speed control block diagram used in ECU. The most effective operating range of the engine was between rated speed 1500rpm and peak speed 6000rpm. The parameters of the Genset are tabulated in Table 3. The Genset system (Fig 17) is used to charge the battery. When the battery packs state-of-charge (SOC) is too low (SOC<45%) to support pure EV operation the Genset system is turned on. Genset system provides the power to charge the battery and maintain the batteries at an acceptable SOC otherwise to prove motor drive power at the same time.

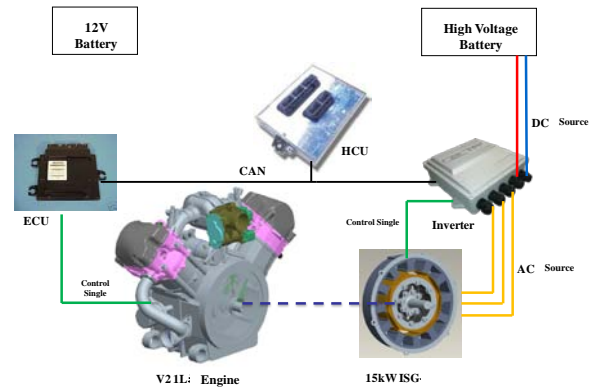


Figure16: ICE/generator power and speed control block diagram



Figure17: Genset system

Table3: Parameters of the ICE

| | Genset series | RE-15 |
|--------------------------------|------------------------|------------------|
| Range extender specification | Rated power (kW) | 15 |
| | Rated speed (rpm) | 1500 |
| | Rated BSFC (g/kWh) | 260 |
| | Peak power (kW) | 25 |
| | Peak power speed (rpm) | 2500 |
| IC Engine specification | Voltage (V) | 220-450 |
| | Fuel type | Petro, Octane 92 |
| | Type | V2, 4 stroke |
| | Valvetrain | SOHC 4V |
| | Displacement (c.c.) | 998.6 |
| | Bore/Stroke (mm) | 86 / 86 |
| | Compression ratio | 10 |
| | Fuel system | MPFI |
| | Throttle | ETC |
| | Max. power (kW) | 41.3 |
| Generator specification | Max. power speed (rpm) | 6000 |
| | Emission | EURO V |
| | Cooling type | Water cooled |
| | Type | PMSM |
| | Rated power (kW) | 15 |
| Generator driver specification | Rated speed (rpm) | 1500 |
| | Peak power (kW) | 25 |
| | Peak power speed (rpm) | 2500 |
| | Max. speed (rpm) | 6000 |
| | Rated Torque (Nm) | 95 |
| | Peak Torque (Nm) | 159 |
| | Generator cooling type | Oil+Water cooled |
| Generator driver specification | Peak Power | 30kW |
| | Operating Voltage | 100V - 400V |
| | Maximum Current | 300A |
| | Driving Algorithm | Vector Control |
| | Motor type support | PM |
| | MCU | 32 bit |
| | Power electronics | Module IGBT |
| Cooling | Liquid cooled | |
| Position Feedback | Resolver+Hall Sensor | |

7 Simulation Result

A forward simulation model is established for the vehicle under MATLAB/Simulink environment. Driver module passes acceleration and brake pedal signals to the vehicle controller according to the request speed (cycle speed) and the vehicle speed. According to the pedal signals, vehicle controller uses the control strategy to split the power instantaneously. Vehicle speed information is given by the vehicle module and feedbacks to the driver and vehicle controller. The proposed methodology allows for the calculation of the torque and speed controller commands in time, which maximizes the total system efficiency while producing the requested target energy in a requested time interval. The first case examines the vehicle on acceleration, and deceleration the results are shown in Figure 18 and 19. From the Figure 18 and 19, the vehicle can reasonably track the desired velocity (120kph). It has also shown that the SOC is higher than 45%. In this mode, only the battery is working to accelerate the vehicle. It can be seen that the SOC and battery voltage increases during deceleration period that is also one of the important factors in range extended electric vehicle designs to regenerate the power.

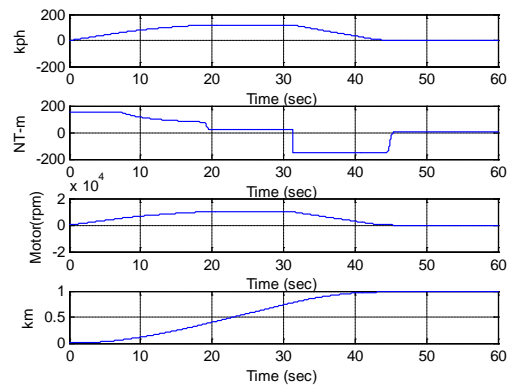


Figure18: Acceleration and deceleration test I

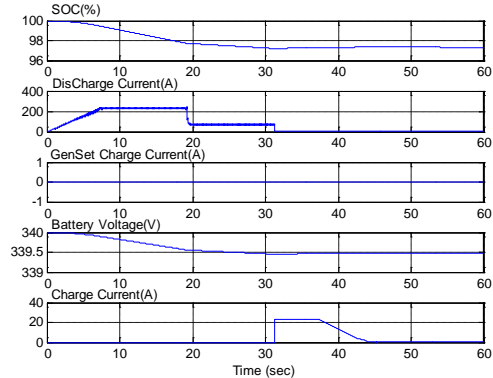


Figure19: Acceleration and deceleration test II

By a highway-like driving (vehicle speed reaching 100 kph) are show in Figure 20 and 21. The Genset system will always be ON (SOC<50%), if the driver demand is to cruise the vehicle at high speed and make the battery was operated at a balance SOC =45%.

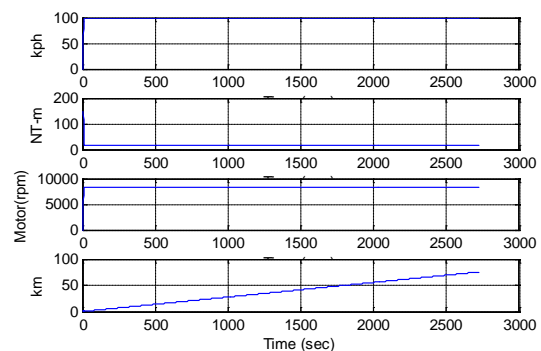


Figure20: Highway-like driving test I (100kph)

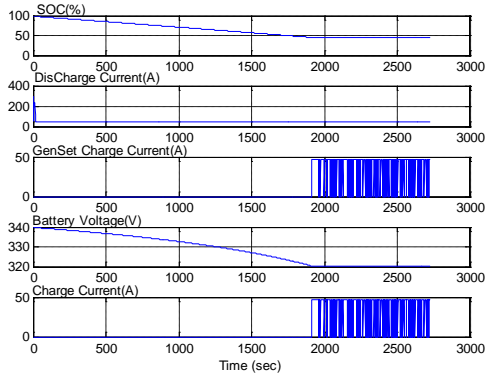


Figure 21: Highway-like driving test II (100kph)

The Figure 22 and 23 are a random desired vehicle velocity that includes the sharp accelerations and decelerations. The vehicle decelerates and the Genset is not operating. The battery is being recharged due to regenerative braking.

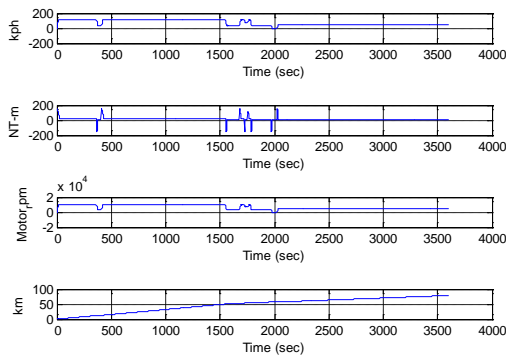


Figure 22: Random desired vehicle velocity test (I)

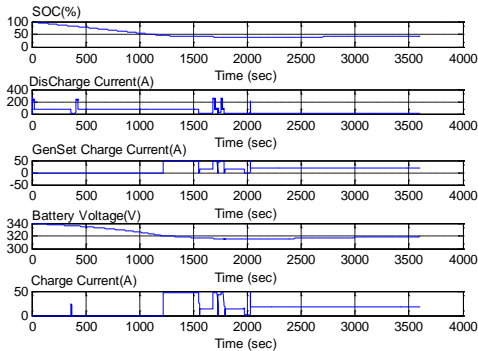


Figure 23: Random desired vehicle velocity test (II)

8 Conclusion

This paper presents the modeling and control of a new power flow control strategy for a variable speed engine-generator based range-extended electric vehicle. In this paper, structure of range

extended electric vehicle was shown; optimum Genset control strategy and electric-assisted control strategy were analyzed and compared. The goal of this paper was to obtain a complete and optimum control structure for the studied range extended electric vehicle. Numerical models of battery and transmission were established. In order to check the model and control of the studied system, a simple strategy is taken into account and discussed the programs were written base on these theories. At the end of this paper, simulation results were analyzed, and it has been proved that range extended electric vehicle can avoid deep discharge cycles. Therefore, range extended electric vehicle battery cycle life definitely greater than EV battery cycle life. It's also meaning that battery operating cost of range extended electric vehicle being much lower than EV.

References

- [1] Q. Gong, Y. Li and Z. R. Peng, *Trip-Based Optimal Power Management of Plug-in Hybrid Electric Vehicles*, IEEE Transactions on Vehicle Technology, 57(2008), 3393-3410
- [2] P. Fajri and B. Asaei, *Plug-in Hybrid Conversion of a Series Hybrid Electric Vehicle and Simulation Comparison*, Optimization of Electrical and Electronic Equipment, 287-292, 2008
- [3] S. Neglur and M. Ferdowsi, *Effect of Battery Capacity on the Performance of Plug-in Hybrid Electric Vehicles*, Vehicle Power and Propulsion Conference, 649-654, 2009
- [4] C. E. N. Baron, A. R. Tariq, G. Zhu and E. G. Strangas, *Trajectory Optimization for the Engine-Generator Operation of a Series Hybrid Electric Vehicle*, IEEE Transactions on Vehicular Technology, 60(2011), 2438-2447
- [5] H. Yoo, B. G. Cho, S. K. Sul, S. M. Kim and Y. Park, *A Power Flow Control Strategy for Optimal Fuel Efficiency of a Variable Speed Engine-Generator based Series Hybrid Electric Vehicle*, Energy Conversion Congress and Exposition, 443-450, 2009
- [6] X. Liu, Y. Wu and J. Duan, *Optimal Sizing of a Series Hybrid Electric Vehicle Using a Hybrid Genetic Algorithm*, IEEE International Conference on Automation and Logistics, 1125-1129, 2007
- [7] A. F. Burke, *Batteries and Ultracapacitors for Electric, Hybrid, and Fuel Cell Vehicles*, Proceedings of the IEEE , Vol. 95, No. 4, April 2007.

- [8] A. Lorico, J. Taiber, and T. Yanni, *Effect of Inductive Power Technology Systems on Battery-Electric Vehicle Design*, Proceedings of the Annual Conference on IEEE Industrial Electronics Society, Vol. 37, 2011.
- [9] J. P. Trovão, P. G. Pereirinha and F. J. T. E. Ferreira, *Comparative Study of Different Electric Machines in the Powertrain of a Small Electric Vehicle*, Proceedings of the 2008 International Conference on Electrical Machines, Vol. 18, 2008.
- [10] D. M. Sousa, A. Roque and C. Casimiro, *Analysis and Simulation of a System Connecting Batteries of an Electric Vehicle to the Electric Grid*, Proceedings of the 2011 International Conference on Power Engineering, Energy and Electrical Drives, 2011.

Authors



Chang Chih-Ming is an Assistant Chief of Vehicle Structure & System Section in Metal Industries R&D Centre. Graduate in Mechanical and Automation Engineering Department of National Kaohsiung First University of Science and Technology.



Kuang-Shine Yang received the M.S. degrees in National Pingtung University of Science and Technology, in 2004 and 2006, respectively, Pingtung, Taiwan, and is currently working toward the Ph.D degree in mechanical engineering from National Sun Yat-sen University, Kaohsiung, Taiwan.